OPTICAL IMAGE PROCESSING

Effect of the parameters of a wide-aperture acousto-optic filter on the image processing quality

V.B. Voloshinov, D.V. Bogomolov

Abstract. **The properties of wide-aperture paratellurite crystal acousto-optic filters used for optical image processing are studied. The influence of parameters of these filters on the quality of optical imaging in laser and nonmonochromatic light is studied. The spatial resolution of filters is measured upon laser and nonmonochromatic illumination of objects. Filtration is performed in a broad wavelength range at different powers of a control electric signal. The optimisation of the filter parameters for improving its spatial resolution is discussed.**

Keywords: *wide-aperture acousto-optic filter, image quality, spatial resolution.*

1. Introduction

It is known that tunable acousto-optic (AO) filters used for image analysis provide a great body of information on the objects under study. Information can be obtained in real time upon illumination both by monochromatic and nonmonochromatic light [1]. For example, AO filters using laser beams can be applied in optoelectronic systems of pattern recognition, artificial vision, image correction, devices for parallel data processing, etc. [1 – 5]. In the study of objects emitting nonmonochromatic light or upon illumination of objects by light with a continuous spectrum, AO devices give information on the spectral and polarisation parameters of radiation in the UV, visible, and IR spectral regions.

Because of this, AO filters find at present various applications in many fields of science and technology such as optics and spectroscopy, laser technologies, astronomy, chemistry and medicine, ecological control and remote monitoring of the Earth surface and atmosphere [6 – 29].

In this paper, we studied the influence of the AO interaction on the quality of images obtained at the output of wide-aperture AO filters. The analysis was performed for a paratellurite (TeO₂) crystal filter in which a piezoelectric transducer excited a shear acoustic wave [1, 24, 29]. Due to

V.B. Voloshinov, D.V. Bogomolov Department of Physics, M.V. Lomonosov Moscow State University, Vorob'evy gory, 119992 Moscow, Russia; e-mail: volosh@phys.msu.ru

periodic variations in the refractive index induced by ultrasound, a three-dimensional phase grating with parameters determined by the frequency and power of the control electric signal was produced in the crystal. Image processing was performed by using a wide-aperture interaction geometry in the $(1\bar{1}0)$ plane of the crystal in which a slow shear ultrasonic wave was directed at the angle $\alpha = 10°$ to the [110] axis [6]. The length of the AO filter transducer was $l_0 = 1.2$ cm and the size of the linear optical aperture of the device was 0.6×0.6 cm. The filter was tuned almost over the entire visible range, had a good resolution and high transmission coefficient.

2. Spatial resolution of image processing

It is known that the efficient AO interaction occurs only when the Bragg condition relating the wavelength of light λ, the angle of incidence θ of light on the acoustic wave front, and the ultrasonic frequency f is fulfilled [1]. The expression for the Bragg angle of incidence of light in a birefringent crystal has the form

$$\sin \theta = \frac{\lambda f}{2 n_i V}\left[1 + \frac{V^2}{\lambda^2 f^2}\left(n_i{}^2 - n_d^2\right)\right], \qquad (1)$$

where V is the phase velocity of sound and n_i and n_d are the refractive indices for the incident and diffracted light beams. It follows from (1) that radiation incident on the ultrasonic grating at the Bragg angle is selected at the fixed ultrasonic frequency from an uncollimated monochromatic beam of light directed on an AO filter. The operation of AO spatial frequency filters is based on this principle [25, 26]. If nonmonochromatic radiation is incident on the AO filter, the wavelength λ of light transmitted by the filter is determined by the angle of incidence θ and ultrasonic frequency f. The operation of temporal frequency filters is based on this property [6 – 19, 28].

One of the important characteristics of image processing is the maximum number of resolvable pixels. The spatial resolution of the optical system along the selected direction is determined by the maximum number N of resolvable pixels in the decomposition line:

$$N = \frac{\Delta \theta}{\delta \theta}, \qquad (2)$$

where $\delta \theta$ is the angular size of the minimal resolvable pixel, and $\Delta \theta$ is the angular size of the image as a whole. It is obvious that the minimal angle $\delta \theta$ is restricted by

diffraction [5]. Various factors affecting the quality of a filtered image and determining the spatial resolution of a tunable paratellurite crystal AO filter are considered in monograph [5].

3. Vector relations in the interaction of light with sound

It is known that AO devices can be used as filters of spatial frequencies upon image processing in coherent light. For example, AO filters are employed for image mapping, visualisation of phase objects or real-time integration, differentiation, convolution, etc. [4, 21, 22, 25, 26]. It has been found that it is convenient to study the characteristics of all tunable AO filters, even those operating with nonmonochromatic light, in coherent light.

The maximum angular size $\Delta\theta$ of the image processed with the help of a filter is determined by the angle $\Delta\theta_d$ between the optical beam transmitted through the AO cell and the beam diffracted in it. If the angular aperture of the incident optical beam exceeds the angle $\Delta\theta_d$, the images in the zero and first diffraction orders are spatially overlapped [11]. As a result, these images prove to be coincident, which reduces the signal-to-noise ratio [11]. Therefore, the angular aperture of the AO filter should be restricted by the deflection angle $\Delta\theta_d$, i.e., $\Delta\theta \leqslant \Delta\theta_d$.

To provide the efficient interaction of light with ultrasound, the Bragg phase matching condition should be fulfilled. This condition follows from the law of conservation of momentum upon photon–phonon interaction and can be written in the vector form as $\boldsymbol{k}_i + \boldsymbol{K} = \boldsymbol{k}_d$, where $k_i = 2\pi n_i/\lambda$ and $k_d = 2\pi n_d/\lambda$ are the lengths of the wave vectors of the transmitted and diffracted beams, respectively; $K = 2\pi f/V$ is the length of the acoustic wave vector depending on the phase velocity and frequency of ultrasound. Below, we assume for simplicity that the light beam incident on the acoustic wave front at the Bragg angle has extraordinary polarisation, while the diffracted beam has ordinary polarisation. Then, the refractive index of the paratellurite crystal for diffracted light is $n_d = n_o$, and the refractive index for the incident light is determined from the expression

$$n_i = \frac{n_o n_e}{[n_o^2 \sin^2(\theta+\alpha) + n_e \cos^2(\theta+\alpha)]^{1/2}}, \qquad (3)$$

where n_o and n_e are the refractive indices of the crystal for ordinary and extraordinary optical beams.

From the vector relation $\boldsymbol{k}_i + \boldsymbol{K} = \boldsymbol{k}_d$, we can obtain the expression

$$\Delta\theta_d = \theta - \arccos\left(\frac{n_i}{n_o}\cos\theta\right). \qquad (4)$$

The calculation for paratellurite by expressions (3) and (4) shows that the separation angle $\Delta\theta_d$ of the beams increases with increasing the acoustic cut angle α and achieves its maximum value in air 8.5° for $\alpha = 17.7°$. A further increase in α only slightly reduces $\Delta\theta_d$. It is known that the critical angle at which the AO interaction geometry ceases to be wide-aperture is equal to 18.9° in paratellurite [1, 29].

It is obvious that, if an optical beam is incident at the Bragg angle θ (1), the beam efficiently interacts with ultrasound. If the angle of incidence is not equal to the Bragg angle, the diffraction efficiency decreases due to violation of the phase matching condition. Therefore, monochromatic optical beams can efficiently interact with ultrasound only within some angular range $\Delta\theta^*$ near the Bragg angle θ. It is known that for the specified cut angle α of the crystal, the angle $\Delta\theta^*$ achieves its maximum value if the condition of wide-aperture diffraction $df/d\theta = 0$ is fulfilled [7].

The vector relation for the light incident on the wave front of an acoustic wave at the angle $\theta \pm 0.5\Delta\theta^*$ different from the Bragg angle can be written in the form

$$\boldsymbol{k}_i + \boldsymbol{K} - \boldsymbol{k}_d = \boldsymbol{\eta}, \qquad (5)$$

where $\boldsymbol{\eta}$ is the mismatch vector [1]. Then, the angular aperture of the AO filter can be determined from (5) by solving numerically the system of equations

$$\frac{2\pi n_i}{\lambda}\sin(\theta \pm 0.5\Delta\theta^*) = \frac{2\pi n_o}{\lambda}\sin\theta_d + \frac{2\pi f}{V} + \eta\sin\psi,$$

$$\frac{2\pi n_i}{\lambda}\cos(\theta \pm 0.5\Delta\theta^*) = \frac{2\pi n_o}{\lambda}\cos\theta_d + \eta\cos\psi, \qquad (6)$$

where ψ is the acoustic walkoff angle and $0.5\Delta\theta^*$ is the difference between the angle of incidence of light and the Bragg angle. Therefore, the angle of admissible deviation of light in the AO filter is equal to the doubled angle $\Delta\theta^*$. It is assumed that at the angles of incidence $\theta \pm 0.5\Delta\theta^*$, the intensity of diffracted light decreases by half compared to its intensity when condition (1) is exactly fulfilled. The mismatch η in relation (5) is determined from the obvious inequality $|\eta l_0 \cos\psi| \leqslant 0.8\pi$ [1, 9, 15]. Calculations show that, depending on the cut angle α and the length l_0 of a piezoelectric transducer, the angle of admissible deviation from the Bragg angle for the incident light can be both larger and smaller than the angle of spatial separation $\Delta\theta_d$ of the incident and diffracted beams.

In the approximation of a weakly birefringent crystal $[\Delta n/n_o = (n_e - n_o)/n_o \ll 1]$, taking (1)–(6) into account, the angle of admissible deviation from the Bragg angle is calculated from the expression [24]

$$\Delta\theta^* \simeq \left\{ \frac{3.5\lambda}{\Delta n l_0} \frac{\sin^2(\theta+\alpha)}{2-3\sin^2(\theta+\alpha)}[\tan\psi + \cot(\theta-\Delta\theta_d)] \right\}^{1/2}. \qquad (7)$$

Note that approximate expression (7) has a restricted region of applications and leads to a considerable error for cut angles $\alpha > 18°$. One can see from (7) that the angle $\Delta\theta^*$ decreases with increasing the transducer length l_0. This means that in the general case the decrease in the piezoelectric transducer length leads to the increase in the angular aperture $\Delta\theta^*$ of the filter [17, 24, 29].

As pointed out above, if the angular range $\Delta\theta^*$ exceeds the angle between the transmitted and diffracted beams ($\Delta\theta^* > \Delta\theta_d$), the angular aperture of the AO filter should be restricted by the diffraction angle $\Delta\theta_d$. And vice versa, for $\Delta\theta^* < \Delta\theta_d$, the value of $\Delta\theta^*$ determines the effective angular aperture of the device. Thus, the effective angular aperture $\Delta\theta_{eff}$ of the AO filter is equal to the smallest of the two angles $\Delta\theta_d$ and $\Delta\theta^*$:

$$\Delta\theta_{eff} \simeq \min\left[\Delta\theta_d, \Delta\theta^*\right]. \qquad (8)$$

One can see from expressions (4), (7), and (8) that the required effective angular aperture $\Delta\theta_{\text{eff}}$ in the AO filter can be obtained by choosing appropriately the cut angle of the crystal and optimising the piezoelectric transducer length l_0. For example, for $\alpha = 10°$ and $l_0 = 1.2$ cm, the angle of separation of the beams in air is $\Delta\theta_d = 6.0°$, whereas the angle of admissible deviation is $\Delta\theta^* = 4.0°$. This means that the effective angular aperture of the filter (8) $\Delta\theta_{\text{eff}} = \Delta\theta^* = 4.0°$. Note that the number of resolvable pixels of the image at the filter output depends namely on the effective angular aperture $\Delta\theta_{\text{eff}}$ [4].

4. Number of resolvable pixels of the image upon laser illumination

One of the main reasons restricting the minimal resolvable size of the image in an optical system is the diffraction divergence of optical beams. It is obvious that an AO cell is an optical element with a restricted linear aperture, this aperture being the smallest linear aperture in the filtration system. Therefore, the influence of other elements of the optical system on the resolution can be neglected. Then, by using the Rayleigh criterion for a filter with the linear aperture A illuminated by light at a wavelength of λ, we obtain the angular size of the minimal resolvable pixel of the image [5]

$$\delta\theta \simeq \frac{1.22\lambda}{A}. \tag{9}$$

A high-frequency acoustic wave decays during its propagation in a crystal. Note that in the general case the efficiency of interaction of light and sound depends quadratically on the acoustic wave amplitude [1 – 3]. The effective linear amplitude of the AO cell considerably decreases with increasing acoustic frequency because the acoustic wave amplitude exponentially decreases with distance from the transducer. It is obvious that the image of a light source will be described by the Fourier transform of the function describing the sound intensity distribution over the filter aperture [5]. In the absence of decay of ultrasound, the distribution of the acoustic wave amplitude along the filter aperture is rectangular. In the case of decay of ultrasound, it is convenient to introduce the correction coefficient γ for determining the effective angular size of the minimal resolvable pixel. This coefficient shows to what extent the effective linear aperture of the filter decreases and the angular range $\delta\theta_{\text{m}} = \gamma\delta\theta$, in which the minimal resolvable pixel of the image is contained, increases. One can see from (2) and (9) that the effective angular size of the minimal resolvable pixel depends on the wavelength λ of light and the linear aperture A of the filter.

Thus, by using expressions (2), (8), (9) and taking into account the total decay of the shear acoustic mode in the AO cell equal to 260 dB cm^{-1} GHz^{-2} [2, 3], we can calculate the number N of resolvable pixels in a line of a monochromatic image processed by means of the AO filter:

$$N = \frac{\Delta\theta_{\text{eff}}}{\delta\theta_{\text{m}}}. \tag{10}$$

The calculation shows that the decay of ultrasound in paratellurite of the order of 6 dB cm^{-1} and more affects the spatial resolution of the AO filter. Such a decay is observed in the crystal at ultrasonic frequencies $f > 150$ MHz. For example, the filter operates at $\lambda = 633$ nm with control frequencies $f > 150$ MHz by using crystals with the cut angle $\alpha > 12°$. Because the ultrasonic frequency f increases with decreasing the wavelength of light λ, the number of resolvable pixels in AO devices with the cut angle $\alpha > 10°$ begins inevitably to decrease with decreasing the wavelength of light down to the short-wavelength transmission edge of the crystal ($\lambda = 350$ nm).

The ultrasonic decay in the UV spectral range proved to be so strong that the effective AO interaction occurs not over the entire aperture of the cell but only near the piezoelectric transducer. Because the AO interaction efficiency decreases for large cut angles [1], we can conclude that the brightness of processed images in paratellurite filters with large cut angles ($\alpha > 12°$) strongly decreases and the spatial resolution deteriorates. Therefore, to fulfil the requirements to AO filtration systems, it is necessary to optimise the parameters of AO cells taking into account the values of the angular aperture, aperture ratio, and spatial resolution of the filter.

The dashed curve in Fig. 1 shows the dependence of the number N of resolvable pixels in a line of the processed image on the wavelength of light λ, calculated for the cut angle of paratellurite $\alpha = 10°$, the transducer length $l_0 = 1.2$ cm, and the linear aperture of the filter $A = 0.6$ cm. One can see that the spatial resolution of the filter at the helium – neon laser wavelength 633 nm is restricted by the number of elements in the decomposition line $N = 560$. Such a spatial resolution proves to be sufficient for most applications.
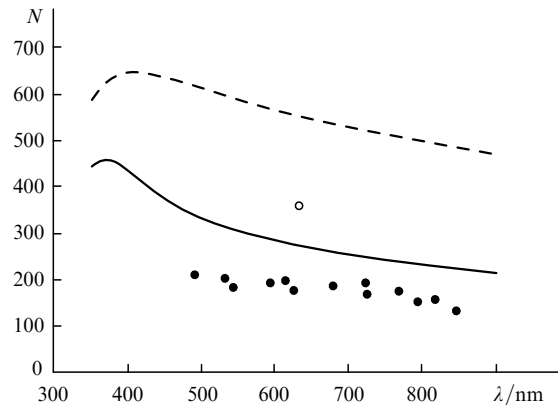
Figure 1. Experimental (circles) and theoretical (curves) dependences of the number of resolvable elements in the image line on the radiation wavelength upon illumination by monochromatic ($\circ$, dashed curve) and nonmonochromatic ($\bullet$, solid curve) light.

5. Number of resolvable pixels of the image upon nonmonochromatic illumination

As follows from the discussion presented above, the quality of processed images upon monochromatic illumination depends on the wavelength of light, the angular aperture of the filter, and ultrasonic decay in a crystal. It was found that upon filtration of nonmonochromatic beams, the maximum number of resolvable pixels in the image decreased compared to that in the case of monochromatic illumination [16, 24, 29].

It is known that AO filters select from a light flux with a continuous spectrum the radiation at the wavelength λ and also with close wavelengths $\lambda \pm \Delta\lambda$ within the transmission band $2\Delta\lambda$ of the filter. The vector relations for light beams with wavelengths $\lambda \pm \Delta\lambda$ are written in the same form (5) as in the monochromatic case. However, if two beams with wavelengths λ and $\lambda - \Delta\lambda$ are incident on the filter in the same direction, the diffracted beam at the wavelength $\lambda - \Delta\lambda$ is deflected by the angle $\delta\theta^*$ from the diffracted beam at the wavelength λ. Therefore, optical beams at different wavelengths are deflected through different angles at the filter output.

We calculated the transmission band $2\Delta\lambda$ of the filter and the deflection angle $2\delta\theta^*$ of nonmonochromatic optical beams from the system of equations

$$\frac{2\pi n_i}{\lambda - \Delta\lambda}\sin\theta = \frac{2\pi n_o}{\lambda - \Delta\lambda}\sin(\theta_d + \delta\theta^*) + \frac{2\pi f}{V} + \eta\sin\psi,$$
(11)
$$\frac{2\pi n_i}{\lambda - \Delta\lambda}\cos\theta = \frac{2\pi n_o}{\lambda - \Delta\lambda}\cos(\theta_d + \delta\theta^*) + \eta\cos\psi,$$

where the diffraction angle θ_d can be found from the relation $n_o\cos\theta_d = n_i\cos\theta$ corresponding to the wavelength λ of light upon phase matching. The transmission band of the AO filter and the deflection angle of light obtained from the system of equations (11) are

$$2\Delta\lambda = \frac{0.8\lambda V}{f l_0}(\cot\theta_d + \tan\psi),$$
(12)

and

$$2\delta\theta^* = \frac{0.8\lambda}{n_o l_0 \sin\theta_d},$$
(13)

respectively.

One can see from (12) that the spectral resolution of the device depends on the piezoelectric transducer length l_0. On the other hand, it follows from (13) that the broadening angle $2\delta\theta^*$ of nonmonochromatic light beams also depends on the transducer length. Therefore, upon the AO interaction of a plane nonmonochromatic optical wave with an acoustic wave, the angular interval of the diffracted beam is determined by the angle $2\delta\theta^*$ (13).

Thus, the spatial resolution in the processed image depends on the diffraction divergence (9) and angular broadening (13) of the beams forming an individual element of the image in nonmonochromatic light. Therefore, the minimal resolvable pixel of the filtered nonmonochromatic image consists of a set of individual elements appearing in monochromatic light with the angular resolution $\delta\theta$, which are spatially oriented within the angle $2\delta\theta^*$. Then, we can assume that the angular size of an individual fragment of the filtered image in the AO interaction plane is $\delta\theta_N = 2\delta\theta^*\gamma^*$, where the correction factor γ^* is calculated from the Rayleigh criterion taking into account the diffraction divergence of light and ultrasonic decay: $\gamma^* \simeq 1$ for $\delta\theta_m \ll 2\delta\theta^*$ and $\gamma^* > 1$ for $\delta\theta_m \geqslant 2\delta\theta^*$. In this case, the angular size $\delta\theta_N$ of the image element formed in nonmonochromatic light depends on the angular size of the image element formed in monochromatic light and always exceeds the latter. As a result, the number of resolvable pixels in the line of the processed nonmonochromatic image is

$$N = \frac{\Delta\theta_{\text{eff}}}{\delta\theta_N}.$$
(14)

It follows from (14) that, depending on the selected values of the acoustic cut angle α, piezoelectric transducer length l_0, and linear aperture A, the maximum number N of resolvable pixels depends in a complicated way on the wavelength λ of filtered radiation. This dependence for nonmonochromatic light calculated for a filter with $\alpha = 10°$, $l_0 = 1.2$ cm, and $A = 0.6$ cm is shown by the solid curve in Fig. 1. One can see that the spatial resolution of the filter N at $\lambda = 633$ nm is restricted by the number $N = 280$. Note that the spatial resolution in nonmonochromatic light decreases compared to that in monochromatic light in the image plane in the propagation direction of ultrasound in the crystal. In this case, the resolution in orthogonal direction is mainly restricted by the effective angular aperture and diffraction divergence, i.e., by the number of elements formed in monochromatic light.

6. Experimental study of the spatial resolution

The experimental setup was assembled according to a standard AO image processing scheme [5, 23, 26]. Radiation from a point source was collimated and directed on a test object consisting of a set of optical test patterns. Behind the point source, an objective and a filter located in the focal plane of the objective were mounted. The radiation diffracted in the AO filter was directed to a receiving digital camera. The test patterns were arranged vertically, horizontally, and at angles $45°$ to the propagation direction of ultrasound in the AO cell. The spatial resolution was studied in diffracted radiation in the plane orthogonal to the incident light. To avoid the overlap of images in the zero and first diffraction orders, the convergence angle of the beam incident on the AO filter was restricted by an iris diaphragm. The filter provided the spectral selection of optical signals in the wavelength range from 460 to 900 nm and in the band $\Delta\lambda = 16$ Å for $\lambda = 630$ nm. The detected images were processed and stored in the PC memory. Note that our experimental scheme provided a magnified image of an object, which allowed us to detect small fragments of the image and to determine the spatial resolution of the wide-aperture AO filter.

The first step in the investigation of the spatial resolution of the filter was analysis of the image of a test pattern obtained upon monochromatic illumination. We used a 633-nm helium–neon laser as a monochromatic radiation source. The test pattern images observed in coherent light had a rather good quality and contained many resolvable pixels. The measurements showed that the AO filter provided about 360 resolvable pixels within the angular aperture $\Delta\theta_{\text{eff}} = 4.0°$ in the image line with a high contrast. The open circle in Fig. 1 shows the spatial resolution of the AO filter measured in coherent light. In addition, we found that the spatial resolution along different directions with respect to the propagation direction of ultrasound was approximately the same. This is explained by the fact that the linear and angular sizes of the filter aperture along the selected directions in paratellurite were approximately the same (0.6×0.6 cm and $4.0° \times 3.5°$, respectively). Figure 2a illustrates the image of a test pattern fragment obtained in the 633-nm coherent light.

The second step of the experimental study was analysis of the images obtained in nonmonochromatic light. The test
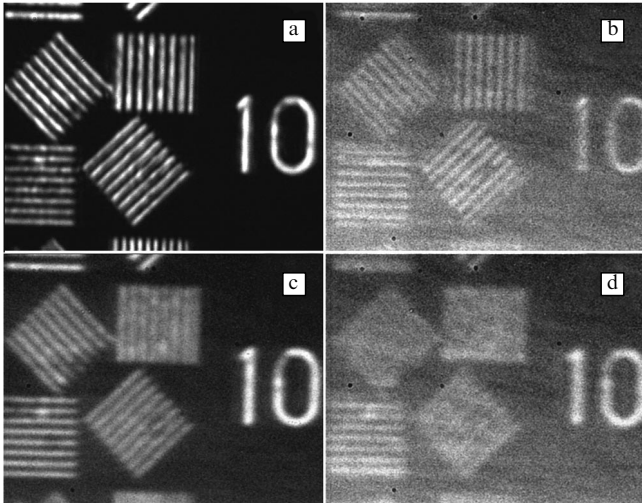
Figure 2. Images of a fragment of the test pattern in the 633-nm coherent light (a) and in incoherent light at 480 (b), 620 (c), and 790 nm (d).

Figure 3. Images of a fragment of the test pattern at control signal powers $P = 0.8$ (a), 0.18 (b), 0.3 (c), and 0.5 W (d).

object was illuminated with an incandescent lamp; in this case, the filter provided image processing at a specified wavelength virtually over the entire visible range. The measurements showed that the quality of processed images, as predicted by the theory, was noticeably worse than that upon monochromatic illumination. For example, images in Figs 2b–d were recorded upon nonmonochromatic illumination at $\lambda = 480$, 620, and 790 nm.

One can see from Fig. 2 that in the horizontal direction corresponding to the propagation direction of ultrasound in the AO cell the spatial resolution is considerably lower than the resolution in monochromatic light. The resolution along the propagation direction of ultrasound at each wavelength was lower by a factor of 1.5 than in the orthogonal direction. In addition, in accordance with the theory, the image quality considerably changed upon tuning the radiation wavelength λ, as illustrated in Fig. 2. The experiment showed that the spatial resolution in nonmonochromatic light along the propagation direction of ultrasound (dark circles in Fig. 1) was limited by the number of elements $N = 120 - 210$.

We also found that the quality of processed non-monochromatic images substantially depended on the control signal power. It is known that the shape of the transmission function of an AO filter depends on the ultrasonic intensity in the cell [1]. When the ultrasonic intensity exceeds the optimal value and the AO interaction efficiency begins to decrease with respect to the maximum value 100 %, the spectral transmission band $2\Delta\lambda$ of the filter broadens. This inevitably results in the increase in the size $\delta\theta_N$ of a minimal resolvable pixel of the image, according to relations (13) and (14). Figure 3 shows the images of a fragment of the test pattern obtained at different control signal powers P at $\lambda = 620$ nm. One can see that, when the control power exceeds the optimal value ($P > 0.2$ W), the processed image becomes substantially distorted and the spatial resolution of the filter decreases.

7. Optimisation of the filter characteristics

Our experimental studies have demonstrated good agreement with the theory, which allows us to analyse the main
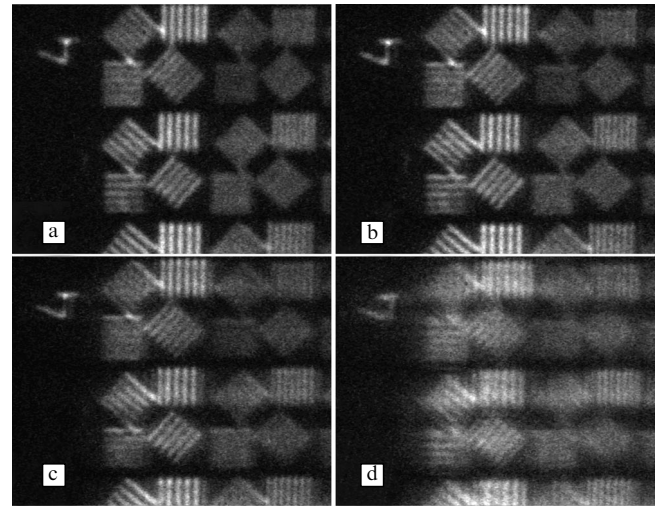
parameters of the AO cell to optimise the filter characteristics. As shown above, the main characteristics of the AO filter depend on the acoustic cut angle α of the crystal determining the geometry of the AO interaction in paratellurite.

Figure 4 presents the dependences of the spatial resolution N on the angle α, calculated for the AO cell with the transducer length $l_0 = 1$ cm and the linear aperture $A = 0.6$ cm. Curves (1) and (2) correspond to monochromatic and nonmonochromatic illumination at $\lambda = 630$ nm, respectively. One can see that curves (1) and (2) have three different regions with two break points. The beaks in the curves correspond to the condition $\Delta\theta^* = \Delta\theta_d$. Therefore, the position of the break points depends on the length l_0 and the wavelength λ. In the first region ($0 < \alpha < 6.2°$), the spatial separation angle $\Delta\theta_d$ of the beams is greater than the angular transmission band $\Delta\theta^*$ of the filter. Therefore, the beam separation angle $\Delta\theta_d < 4.0°$ restricts the effective angular aperture of the filter. On the other hand, a weak selectivity of the AO interaction determines a broad spectral transmission band of the filter ($2\Delta\lambda > 50$ Å) and relatively
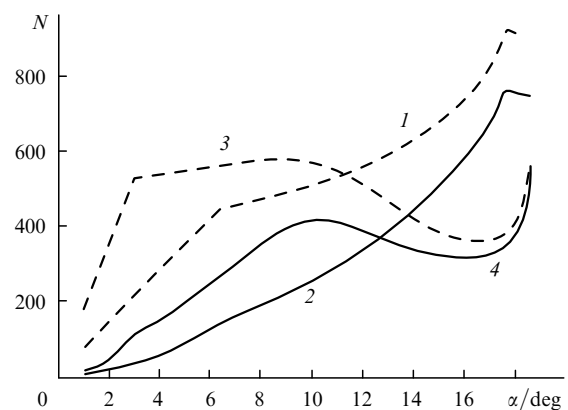
Figure 4. Dependences of the spatial resolution of the AO filter on the cut angle of the crystal upon illumination by monochromatic light at 633 (1) and 360 nm (3) and by nonmonochromatic light at 630 (2) and 360 nm (4).

large angular dimensions of the resolvable image element in nonmonochromatic light ($\delta\theta_N \approx 2\delta\theta^*$). Thus, the spatial resolution in nonmonochromatic light is low ($N < 130$), whereas in coherent light it is restricted by the number $N < 440$.

The second region in Fig. 4 is located within the cut angle $6.2° < \alpha < 17.6°$. The interaction selectivity in this region considerably increases. The beam deflection angle $\Delta\theta_d$ proves to be greater than the angle of admissible deviation $\Delta\theta^*$, and the effective angular aperture is $\Delta\theta_{eff} = \Delta\theta^*$. However, due to the narrowing of the spectral filtration band, angles $\delta\theta_N$ considerably narrow down with increasing α. Note that for $\alpha > 14°$, the broadening angle $2\delta\theta^*$ (13) of nonmonochromatic beams becomes smaller than the diffraction divergence angle $\delta\theta$, i.e., $\delta\theta_N \sim \delta\theta$.

The third region of cut angles (Fig. 4) lies within the limits $17.6° < \alpha < 18.9°$. In this region, the angular size $\delta\theta_N$ of the minimal resolvable pixel and the effective angular size $\Delta\theta_{eff}$ are virtually independent of the cut angle α because $\delta\theta_N \sim \delta\theta_m$ and $\Delta\theta_{eff} = \Delta\theta_d$. Therefore, the spatial resolution of the AO filter will be also independent of the angle α. The calculations show that for $\alpha = 17.8°$ the number of resolvable pixels in the image line achieves the maximum value $N \approx 920$ for monochromatic light and $N \approx 750$ for nonmonochromatic light. This cut angle corresponds to the maximum separation angle of the beams in paratellurite $\Delta\theta_d = 8.5°$. Thus, one can see from the data in Fig. 4 that the spatial resolution of images processed in nonmonochromatic light increases with increasing the acoustic cut angle α and approaches the resolution in monochromatic light.

Curves (3) and (4) in Fig. 4 show the dependences of the spatial resolution of the filter on the cut angle for monochromatic and nonmonochromatic light at $\lambda = 360$ nm, respectively. One can see that for $\alpha < 9°$, the resolution at $\lambda = 360$ nm noticeably increases compared to that at $\lambda = 630$ nm. The spatial resolution noticeably decreases at large cut angles, and for $\alpha > 10° - 12°$ this resolution proves to be worse than at $\lambda = 630$ nm. The predicted behaviour is explained by the influence of ultrasonic decay in the crystal on the effective linear aperture of the AO filter.

Another important factor of the AO filter is the length l_0 of the piezoelectric transducer determining the selectivity of the AO interaction. Figure 5 presents the dependences of the spatial resolution N of the filter in nonmonochromatic light on the length l_0, calculated for $\lambda = 633$ nm and different cut angles α of the crystal. One can see that the spatial resolution achieves maxima at some lengths l_0. The breaks in the curves correspond to the condition $\Delta\theta_d = \Delta\theta^*$. A further increase in the transducer length above its optimal value is accompanied by a decrease in the spatial resolution. This deterioration of the image quality occurs because the size $\delta\theta_N$ of the resolvable image element is restricted by the diffraction divergence angle $\delta\theta$, whereas the effective angular size of the image decreases: $\Delta\theta_{eff} = \Delta\theta^*$. Therefore, for each cut angle of the crystal, the optimal length of the piezoelectric transducer can be calculated by the method proposed at which the maximum spatial resolution of the filter is achieved.
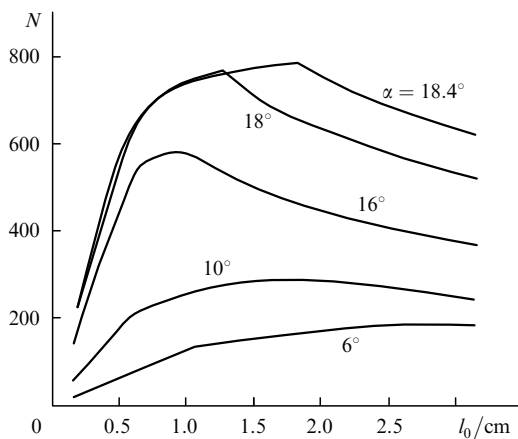
Thus, the spatial resolution of the filter is determined, along with other parameters, by the linear aperture of the AO device. One can see from relations (12) and (13) that the resolution of images in monochromatic light is directly proportional to the linear aperture of the AO cell. However, the size $\delta\theta_N$ of the minimal image element in monochromatic light depends not only on the diffraction divergence $\delta\theta$ of the beams but also on the broadening angle $2\delta\theta^*$. As a result, an increase in the linear aperture A of the filter upon processing nonmonochromatic images may not lead to an increase in the resolution N. Therefore, the optimal linear aperture of the AO filter should be determined from the condition $\delta\theta_N = \delta\theta_m$. In this case, the value of A proves to be dependent on the cut angle α, the transducer length l_0, and the wavelength of light λ.

8. Conclusions

Our theoretical and experimental studies have shown that the spatial resolution of AO filters depends on the angular and linear dimensions of the filter aperture and the interaction wavelength of light and ultrasound. The calculation has shown that the spatial resolution of the TeO$_2$ crystal filter with the acoustic cut angle $\alpha = 10°$, the transducer length $l_0 = 1.2$ cm, and the 0.6×0.6-cm linear aperture upon image processing in the 633-nm monochromatic light is $N \leqslant 560$ in the decomposition line. However, upon filtration of nonmonochromatic images, the resolution of the AO filter considerably decreases to $N \leqslant 280$. This means that the spatial resolution of processed images is determined by the spectral resolution of the AO filter.

The number of resolvable pixels obtained in experiments with coherent light was $N \approx 360$. The difference between the experimental and theoretical data is explained by the inhomogeneous distribution of the ultrasonic field in the crystal and by distortions appearing due to the angular selectivity of the filter. Similar measurements in nonmonochromatic light have shown that images contained ~ 190 elements in the decomposition line. In addition, the experiment has shown that the spatial resolution upon filtration depends on the radiation wavelength λ and increases in the UV region. We also have shown that, depending on the tuning range of the filter and requirements to the aperture ratio of the device, it is necessary to select a proper acoustic cut angle of the crystal and to optimise the dimensions of the transducer of the AO cell and its linear aperture.

Figure 5. Dependences of the spatial resolution of the AO filter on the piezoelectric transducer length at different cut angles of the crystal.

References

1. Balakshy V.I., Parygin V.N., Chirkov L.E. *Fizicheskie osnovy akustooptiki* (Physical Fundamentals of Acousto-optics) (Moscow: Radio i Svyaz', 1985).

2. Xu J., Stroud R. *Acousto-Optic Devices* (New York: Wiley, 1992).

3. Goutzoulis A., Pape D. *Designing and Fabrication of Acousto-Optic Devices* (New York: Marcel Dekker Inc., 1994).

4. Parygin V.N., Balakshy V.I. *Opticheskaya obrabotka informatsii* (Optical Data Processing) (Moscow: Moscow State University, 1987).

5. Goodman J. *Introduction to Fourier Optics* (New York: McGraw Hill, 1968).

6. Chang I.C. *Proc. SPIE Int. Soc. Opt. Eng*, **90**, 12 (1976).

7. Chang I.C. *Opt. Eng*., **20**, 824 (1981).

8. Glenar D.A., Hillman J.J., Saif B., et al. *Appl. Opt*., **33**, 7412 (1994).

9. Voloshinov V.B. *Proc. SPIE Int. Soc. Opt. Eng*., **3584**, 141 (1998).

10. Belikov I.B., Buimistryuk G.Ya., Voloshinov V.B., et al. *Pis'ma Zh. Tekh. Fiz*., **10**, 1225 (1984) [*Tech. Phys. Lett*.., **10**, 1225 (1984)].

11. Voloshinov V.B., Mironov O.V., Trotz E.V. *Opt. Spektrosk*., **71**, 526 (1991) [*Optics and Spectroscopy*, **71**, 306 (1991)].

12. Voloshinov V.B., Mironov O.V., Molchanov V.Ya., et al. *Pis'ma Zh. Tekh. Fiz*., **15**, 69 (1989) [*Tech. Phys. Lett*.., **15**, 69 (1989)].

13. Voloshinov V.B., Mironov O.V. *Opt. Spektrosk*., **68**, 452 (1990) [*Optics and Spectroscopy*, **68**, 264 (1990)].

14. Gupta N., Voloshinov V. *Appl. Opt*., **43** (13), 2752 (2004).

15. Voloshinov V.B., Gupta N. *Proc. SPIE Int. Soc. Opt. Eng*., **3900**, 68 (1999).

16. Suhre D.R., Gottlieb M., Taylor L.H., et. al. *Opt. Eng*., **31**, 2118 (1992).

17. Pozhar V.E., Pustovoit V.I. *Photonics and Optoelectronics*, **4** (2), 67 (1997).

18. Voloshinov V.B., Molchanov V.Ya., Mosquera J.C. *Opt. Laser Technol*., **28** (2), 119 (1996).

19. Georgiev G., Glenar D.A., Hillman J.J. *Appl. Opt*., **41** (1), 209 (2002).

20. Voloshinov V.B., Parygin V.N., Molchanov V.Ya. *Proc. SPIE Int. Soc. Opt. Eng*., **4353**, 17 (2001).

21. Voloshinov V.B., Babkina T.M. *J. Pure Appl. Opt*., **3** (4), S54 (2001).

22. Voloshinov V.B., Molchanov V.Ya., Babkina T.M. *Opt. Eng*., **41** (6), 1273 (2002).

23. Voloshinov V., Gupta N. *Appl. Opt*., **43** (19), 3901 (2004).

24. Bogomolov D.V., Voloshinov V.B. *Proc. SPIE Int. Soc. Opt. Eng*., **5828**, 105 (2004).

25. Balakshy V.I., Voloshinov V.B., Babkina T.M., et al. *J. Mod. Opt*., **52** (1), 1 (2005).

26. Balakshy V.I., Voloshinov V.B. *Kvantovaya Elektron*., **35**, 85 (2005) [*Quantum Electron*., **35**, 85 (2005)].

27. Gupta N., Voloshinov V. *Opt. Lett*., **30** (9), 985 (2005).

28. Vila J., Calpe J., Pla F., et al. *Real-Time Imaging*, **11**, 85 (2005).

29. Voloshinov V.B., Bogomolov D.V. *Proc. SPIE Int. Soc. Opt. Eng*., **5953**, 125 (2005).